

# Electric Field Tunable Correlated States and Magnetic Phase Transitions in Twisted Bilayer-Bilayer Graphene

Yuan Cao,<sup>1,\*</sup> Daniel Rodan-Legrain,<sup>1</sup> Oriol Rubies-Bigord,<sup>1</sup> Jeong Min Park,<sup>1,2</sup> Kenji Watanabe,<sup>3</sup> Takashi Taniguchi,<sup>3</sup> and Pablo Jarillo-Herrero<sup>1,†</sup>

<sup>1</sup>*Department of Physics, Massachusetts Institute of Technology, Cambridge, Massachusetts 02139, USA*

<sup>2</sup>*Department of Chemistry, Massachusetts Institute of Technology, Cambridge, Massachusetts 02139, USA*

<sup>3</sup>*National Institute for Materials Science,  
Namiki 1-1, Tsukuba, Ibaraki 305-0044, Japan*

(Dated: December 15, 2024)

The recent discovery of correlated insulator states and superconductivity in magic-angle twisted bilayer graphene<sup>1,2</sup> has paved the way to the experimental investigation of electronic correlations in tunable flat band systems realized in twisted van der Waals heterostructures<sup>3-6</sup>. This novel twist angle degree of freedom and control should be generalizable to other 2D systems, which may exhibit similar correlated physics behavior while at the same time enabling new techniques to tune and control the strength of electron-electron interactions. Here, we report on a new highly tunable correlated system based on small-angle twisted bilayer-bilayer graphene (TBBG), consisting of two rotated sheets of Bernal-stacked bilayer graphene. We find that TBBG exhibits a rich phase diagram, with tunable correlated insulators states that are highly sensitive to both twist angle and to the application of an electric displacement field, the latter reflecting the inherent polarizability of Bernal-stacked bilayer graphene<sup>7,8</sup>. We find correlated insulator states that can be switched on and off by the displacement field at all integer electron fillings of the moiré unit cell. The response of these correlated states to magnetic fields points towards evidence of electrically switchable magnetism. Moreover, the strong dependence of the resistance at low temperature near the correlated insulator states indicates possible proximity to a superconducting phase. Furthermore, in the regime of lower twist angles, TBBG shows multiple sets of flat bands near charge neutrality, resulting in numerous correlated states corresponding to half-filling of each of these flat bands. Our results pave the way to the exploration of novel twist-angle and electric-field controlled correlated phases of matter in novel multi-flat band twisted superlattices.

Electronic correlations play a fundamental role in condensed matter systems where the bandwidth is comparable to or less than the Coulomb energy of the electrons. These correlation effects often manifest themselves as intriguing quantum phases of matter, such as a ferromagnetism, superconductivity, Mott insulators, or fractional quantum Hall states. Understanding, predicting and characterizing these correlated phases is of great interest in modern condensed matter physics research and poses challenges to both experimentalists and theorists. Recent studies in twisted graphene superlattices provide us with an ideal, tunable platform for investigating electronic correlations in two dimensions<sup>1,2,9–11</sup>. Tuning the twist angle of 2D van der Waals heterostructures to realize novel electronic states, an emerging field referred to as ‘twistronics’, has enabled physicists to explore a variety of novel phenomena.<sup>6,9,12–17</sup> When two layers of graphene are twisted by a specific angle, the phase diagram in the system exhibits correlated insulator states with similarities to Mott insulator systems<sup>1</sup>, as well as exotic superconducting states upon charge doping<sup>2,9,10</sup>. These effects likely stem from the many-body interactions between the electrons, when the band structure becomes substantially flattened as the twist angle approaches the first magic angle  $\theta \approx 1.1^\circ$ <sup>3–5</sup>.

Here we extend the twistronics research on twisted bilayer graphene to a new system with electrical displacement field tunability — twisted bilayer-bilayer graphene (TBBG), which consists of two sheets of untwisted Bernal-stacked bilayer graphene stacked together at an angle  $\theta$ , as illustrated in Fig. 1a. Compared to monolayer graphene, the band structure of bilayer graphene is highly sensitive to the applied perpendicular electric displacement field through it<sup>7</sup>, and therefore provides us with an extra knob to control the strength of electronic correlations in the bands. Similar to that of twisted bilayer graphene (TBG)<sup>3–5</sup>, the band structure of TBBG is flattened near  $\sim 1.1^\circ$  (see Fig. 2e-g)<sup>18</sup>. For devices with twist angles near this value, our experiments show that the correlated insulator behavior at half-filling  $n_s/2$  in TBBG can be sensitively turned on and off by the displacement field, where  $n_s$  is the density corresponding to fully filling one spin and valley degenerate superlattice band<sup>19,20</sup>. The correlated insulator states are sensitive to the twist angle, and devices with slightly larger twist angles (e.g.  $1.23^\circ$ ) exhibit a richer phase diagram, with multiple correlated insulating states at quarter fillings of the superlattice,  $\frac{k}{4}n_s$ , where  $k$  is an odd number<sup>2,9,10,13</sup>. On the other hand, devices with smaller twist angles, such as  $0.84^\circ$ , display multiple correlated states at higher fillings, indicating the presence of multiple flat bands in the electronic structure. The combination of twist angle, electric displacement field and magnetic field control therefore provides a rich arena to investigate novel phenomena in the emerging field of twistronics.

We fabricated high-mobility dual-gated TBBG devices with the reported ‘tear and stack’

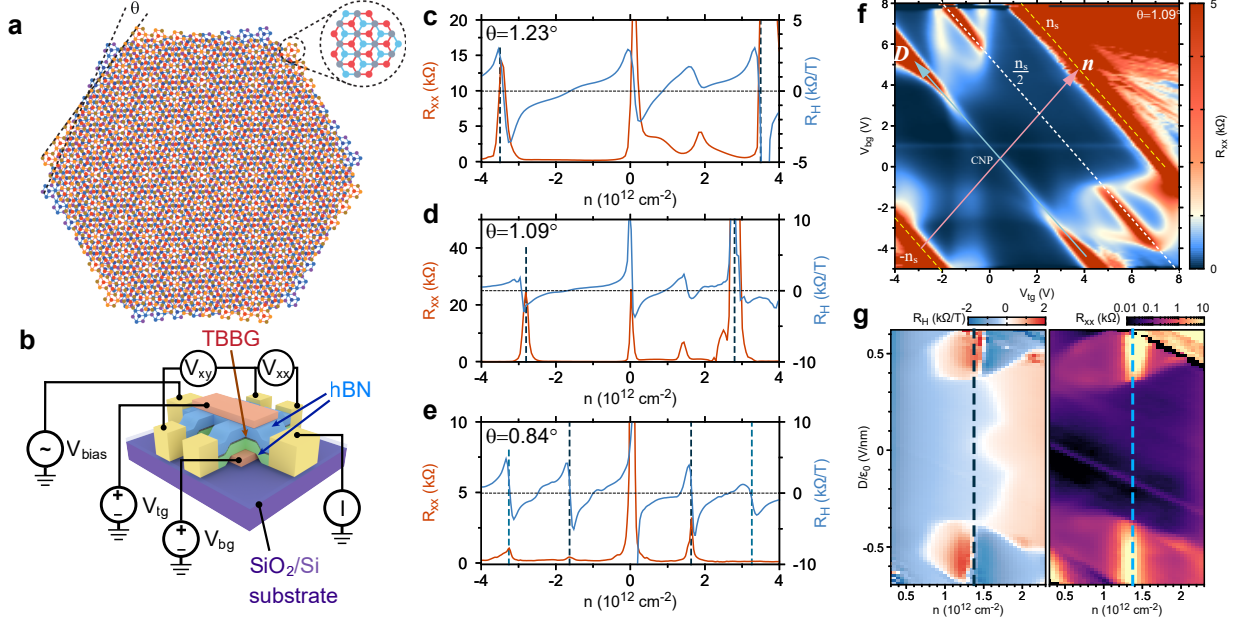


FIG. 1: Structure and transport characterization of twisted bilayer-bilayer graphene (TBBG). (a) TBBG consists of two sheets of Bernal-stacked bilayer graphene twisted at an angle  $\theta$ . (b) Schematic of a typical TBBG device with top and bottom gates and a Hall-bar geometry for transport measurements. (c-e) Measured longitudinal resistance  $R_{xx} = V_{xx}/I$  and low-field Hall coefficient  $R_H = \frac{d}{dB} \left( \frac{V_{xy}}{I} \right)$  as functions of carrier density  $n$  in three devices with twist angles  $\theta = 1.23^\circ$ ,  $1.09^\circ$  and  $0.83^\circ$  respectively. The vertical dashed lines denote multiples of the superlattice density  $n_s$ , where the peaking of  $R_{xx}$  and sign changing of  $R_H$  indicate the Fermi energy crosses a band edge of the superlattice bands. (f) Resistance of the  $1.09^\circ$  TBBG device versus both top gate and bottom gate voltages  $V_{tg}$  and  $V_{bg}$ . The charge density  $n$  and displacement field  $D$  are related to the gate voltages by a linear transformation (see Methods). The superlattice densities  $\pm n_s$  and the half-filling line at  $n_s/2$  are labeled in dashed lines parallel to the  $D$  axis. Correlated insulator states are observed at  $n_s/2$  filling in finite displacement fields. (g) Map of low-field Hall coefficient  $R_H$  (left panel) and resistance  $R_{xx}$  (right panel) near the  $n_s/2$  correlated states for the  $1.09^\circ$  TBBG device. We find that accompanying the onset of the correlated insulator states at  $D/\varepsilon_0 \approx \pm 0.35 \text{ V nm}^{-1}$ , a new sign change of the Hall coefficient also emerges.

method<sup>19,21</sup>, using exfoliated Bernal-stacked bilayer graphene instead of monolayer graphene. We measured the transport properties of five small-angle devices and here we focus on three of the devices with twist angles  $\theta = 1.23^\circ$ ,  $1.09^\circ$  and  $0.84^\circ$  respectively (see Extended Data Figures for other devices). Figures 1c-e show the longitudinal resistance  $R_{xx}$  and low-field Hall coefficient  $R_H = \frac{dR_{xy}}{dB}$  versus charge density for these three devices at  $T = 4 \text{ K}$ . In a superlattice, the electronic band structure is folded in the mini Brillouin zone (MBZ), defined by the moiré periodicity<sup>3</sup>. Each band in the MBZ can accommodate a total charge density  $n_s = 4/A$ , where  $A$  is the size of the moiré unit cell and the prefactor accounts for spin and valley degeneracies<sup>3,18,19</sup>. The experimental results show a sign change of the Hall coefficient  $R_H$  at each multiple of  $n_s$ , indi-

cating the switching of hole-like pockets to electron-like pockets, and peaks in  $R_{xx}$ , indicating the crossing of new band edges (for  $\theta = 0.84^\circ$ , the band edges at  $-n_s$  and  $\pm 2n_s$  may only have small gaps or may even be semi-metallic, and hence do not exhibit prominent peaks in  $R_{xx}$ . See Fig. 2d-f for band structure calculations). The sharpness of the peaks confirms that the devices show relatively low disorder and have well-defined twist angles. In the  $\theta = 1.23^\circ$  and  $\theta = 1.09^\circ$  devices, we observe signatures of newly formed gaps also at  $n_s/2$  when an electrical displacement field is applied perpendicular to the device. While the total charge density  $n = (c_{bg}V_{bg} + c_{tg}V_{tg})/e$  is kept constant, where  $e$  is elementary charge and  $c_{tg}$  and  $c_{bg}$  are top and bottom gate capacitances per area respectively, the electrical displacement field penetrating the sample  $D = (c_{bg}V_{bg} - c_{tg}V_{tg})$  can be altered independently by applying differential gate voltages (see Methods for actual values). Fig. 1f shows the resistance map in the  $V_{tg}$ - $V_{bg}$  space for the  $\theta = 1.09^\circ$  device. The transformation between gate voltages and  $(n, D)$  is given in the Methods section. At  $D = 0$ , no insulating behavior other than the full-filling gaps at  $\pm n_s$  is observed. However, when a displacement field  $D$  is applied in either direction, an insulating state appears at  $n_s/2$  for a range of  $D$ . To demonstrate that this is a new insulator state induced by the displacement field, the Hall coefficient  $R_H$  is mapped out versus  $n$  and  $D$  in Fig. 1g ( $\theta = 1.09^\circ$  device), with  $R_{xx}$  for comparison. At the onset of the insulating states at  $D/\epsilon_0 \approx \pm 0.35 \text{ V nm}^{-1}$ , where  $\epsilon_0$  is the vacuum permittivity,  $R_H$  develops additional sign changes adjacent to the insulating states, suggesting the creation of new gaps by the displacement field. The insulating states disappear when  $D/\epsilon_0$  exceeds  $\pm 0.7 \text{ V nm}^{-1}$ . In both the  $\theta = 1.09^\circ$  device and the  $\theta = 1.23^\circ$  devices, we find signatures of the onset of a correlated state at  $n = -n_s/2, D = 0$  but no well-developed correlated state is observed (see Extended Data Figures).

In the  $\theta = 1.23^\circ$  device, we observe a similar but more intricate hierarchy of tunable insulating states that stem from the interplay of correlations, the superlattice bands, and the magnetic field. Fig. 2a shows the  $n$ - $D$  resistance map of the  $\theta = 1.23^\circ$  TBBG device measured at  $T = 0.07 \text{ K}$ . Noticeably, as  $|D|$  is increased the insulating state at charge neutrality  $n = 0$  strengthens in the same way as in Bernal-stacked bilayer graphene, while the superlattice gaps at  $\pm n_s$  weaken and eventually disappear (for  $|D|/\epsilon_0 > 1.2 \text{ V nm}^{-1}$  for the  $+n_s$  insulating state and for  $|D|/\epsilon_0 > 0.7 \text{ V nm}^{-1}$  for the  $-n_s$  insulating state). The band structures of TBBG in zero and finite external displacement fields calculated using a continuum approximation are shown in Fig. 2e-g (see Methods for details). It should be noted that, although TBBG has twice the number of graphene layers than TBG, the band counting is the same as TBG, *i.e.* each band (spin/valley degenerate) accommodates 4 electrons per moiré unit cell. At zero displacement field, the gap at charge neutrality

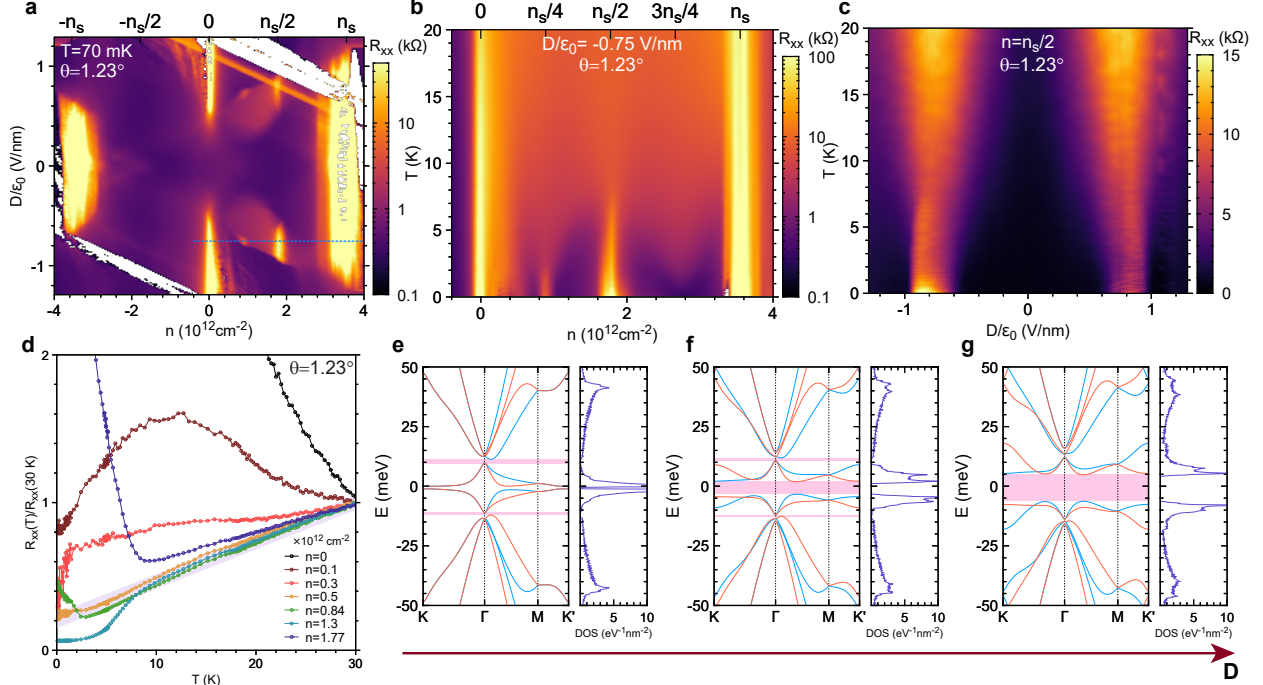


FIG. 2: Displacement field tunable correlated insulator state in TBBG. (a) Colormap of resistance in the  $\theta = 1.23^\circ$  sample versus the charge density  $n$  and the displacement field  $D$ . The blue dashed line cutting through the  $D < 0$  correlated state is the linecut along which (b) is taken. (b) The correlated insulator states at  $n_s/4$  and  $n_s/2$  are suppressed by raising the temperature. (c) Resistance in the  $n_s/2$  correlated insulator state versus displacement field and temperature. The resistance takes maximum at approximately  $D/\varepsilon_0 = \pm 0.8$  V/nm. (d) Normalized resistance curves versus temperature at different densities between 0 and  $n_s/2 \approx 1.77$  cm $^{-2}$ . Away from charge neutrality point, all resistance curves show linear R-T behaviours at above 10 K, with similar slopes (see Extended Data Figures). At around  $n = 1.3 \times 10^{12}$  cm $^{-2}$  in proximity of the correlated state, abrupt drop in resistance around 6 K indicates possible onset of superconductivity. (e-g) Calculated band structure (left panels) and density of states (right panels) of  $\theta = 1.23^\circ$  TBBG at (e)  $\Delta V = 0$ , (f)  $\Delta V = 6$  mV and (g)  $\Delta V = 12$  mV, where  $\Delta V$  is the potential difference between adjacent graphene layers induced by the external displacement field (assumed to be the same between all layers). Single-particle bandgaps in the dispersion are highlighted by pink bars.

( $E = 0$ ) is negligible while the superlattice gaps above and below the flat bands are visible. When the displacement field is increased, the charge neutrality gap quickly widens while the superlattice gaps become smaller and eventually vanish, in agreement with our data.

At intermediate displacement fields around  $D/\varepsilon_0 = -0.75$  V nm $^{-1}$ , we observe not only insulator states at  $n_s/2$  over a wide range of  $D$ , but also at  $n_s/4$  over a smaller range. We attribute these states to a Mott-like mechanism similar to those observed in TBG, which is a result of the Coulomb repulsion of the electrons in the flat bands when each unit cell hosts exactly 1 or 2 electrons, corresponding to  $n_s/4$  and  $n_s/2$  fillings respectively. The  $n_s/4$  state requires a finer tuning of  $D$  to reveal, possibly due to the smaller gap size. This is evident from Fig. 2b, where we show the

resistance versus  $n$  and temperature  $T$  with displacement field  $D/\varepsilon_0$  fixed at  $-0.75$  V/nm. Both states vanish as temperature rises. While the  $n_s/2$  state persists to approximately 8 K, the  $n_s/4$  disappears at less than 3 K, indicating a smaller energy scale associated with the gap. Fig. 3c shows the resistance of the  $n_s/2$  state versus displacement field and temperature. The 'optimal' displacement field is at approximately  $\pm 0.8$  V/nm. As temperature increases, the peak in  $R_{xx}$  not only decreases in value but also broadens in  $D$ . As shown in Fig. 2d, at temperatures higher than 10 K and away from the charge neutrality point, the transport is dominated by linear  $R$ - $T$  behaviour similar to that observed in TBG<sup>2,9,22</sup>. At a carrier density  $n = 1.3 \times 10^{12}$  cm<sup>-2</sup> (lowest blue curve in Fig. 3d), the  $R$ - $T$  curve shows an abrupt drop at around 6 K, saturating at a small, but finite, resistance. While the lowest resistance does not reach zero, possibly due to a series non-superconducting region due to disorder, the shoulder-like sudden drop in resistance near the correlated insulator state is reminiscent of similar superconducting transitions observed in TBG and rhombohedral trilayer graphene<sup>2,9,10,13</sup>, and our data suggest the proximity of our system to a superconducting phase around this charge density.

Figure 3 shows the response of the various correlated states to magnetic fields applied in either perpendicular or in-plane directions with respect to the sample plane. Figures 3a-c show the  $n$ - $D$  maps of the resistance for the  $\theta = 1.23^\circ$  device at  $B = 0$ ,  $B_\perp = 8$  T and  $B_\parallel = 8$  T, respectively. At zero magnetic field we do not observe an insulating state at 3 electrons per unit cell ( $3n_s/4$  filling). Interestingly, at  $B_\perp = 8$  T, the correlated insulator states at  $n_s/4$  and  $n_s/2$  vanish at their original positions around  $D/\varepsilon_0 = -0.75$  V/nm and reappear above and below their original positions at  $B = 0$ , respectively, and a new correlated state appears now at  $3n_s/4$ . Figure 3d shows the evolution of the  $D$ -position of the  $n_s/2$  state as a function of  $B_\perp$ . It can be seen that at around  $B_\perp = 5$  T, the correlated state shifts abruptly from  $D/\varepsilon_0 > -0.95$  V/nm to  $D/\varepsilon_0 < -0.95$  V/nm. This peculiar behaviour might be attributed to a magnetic field induced spin-polarized insulator to valley-polarized metal phase transition at low  $D$  (due to the competition between regular spin Zeeman and valley Zeeman effects), while at high  $D$  we may have a corresponding metal to valley-polarized insulator transition. We note however that another possibility includes mixed spin-valley polarized states at low  $B_\perp$  which turn into valley polarized states at high  $B_\perp$ .

On the other hand, the resistance for all the correlated insulator states increases monotonically in a parallel magnetic field, as shown in Fig. 3e-f. In Fig. 3g we analyzed the evolution of the size of the correlated gaps with in-plane magnetic field by fitting the maximum resistance of the correlated states at "optimal" displacement fields with an Arrhenius behaviour  $e^{-\Delta/2kT}$ , where  $k$  is the Boltzmann constant and  $\Delta$  is the energy gap size. For all three correlated states

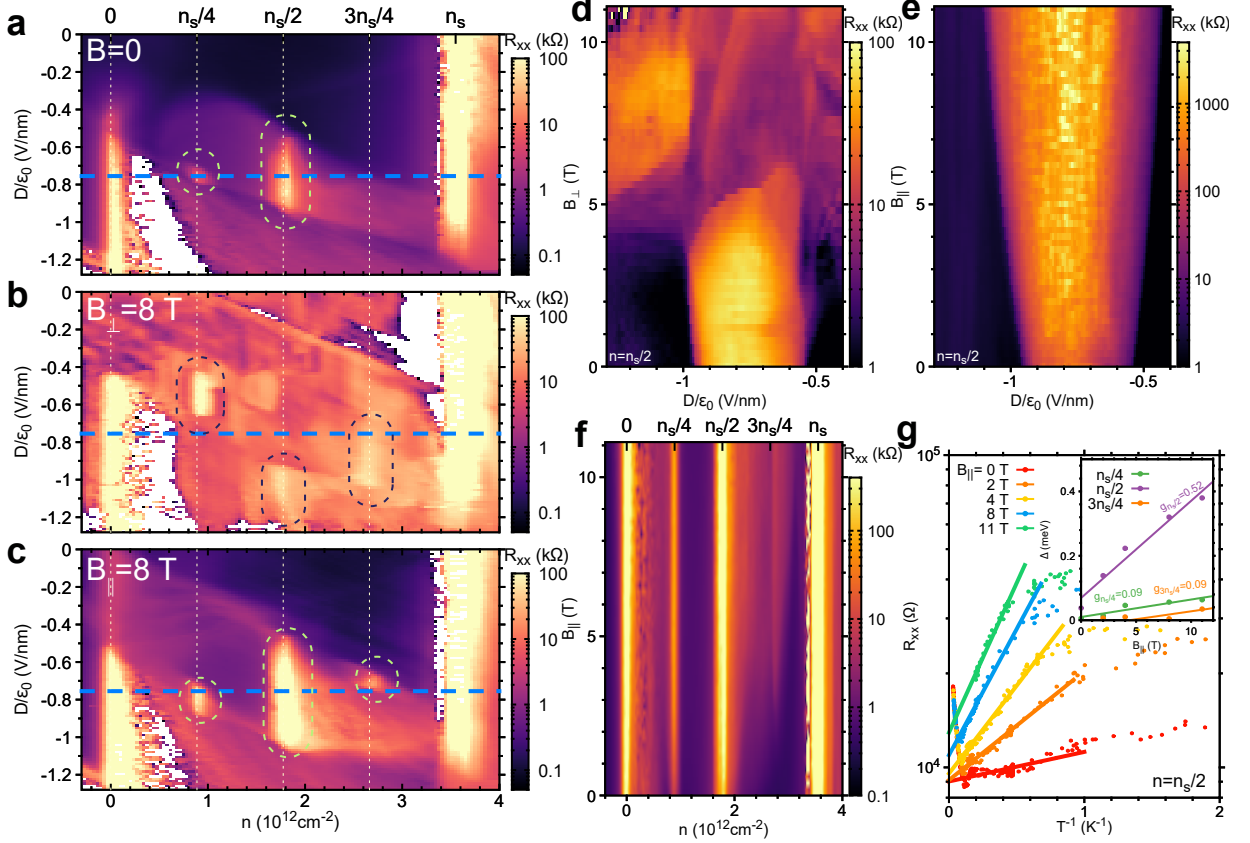


FIG. 3: Magnetic field response of the displacement-field-tunable correlated insulator states in TBGG. (a-c) Resistance map of the  $\theta = 1.23^\circ$  TBGG device in magnetic fields of  $B = 0$ ,  $B_{\perp} = 8$  T perpendicular to the sample, and  $B_{\parallel} = 8$  T parallel to the sample respectively. All measurements are taken at sample temperature  $T = 0.07$  K. Various correlated states at integer electron fillings are indicated by dashed circles. At zero field, only the  $n_s/4$  and  $n_s/2$  states appear around  $|D|/\epsilon_0 = 0.75$  V nm $^{-1}$ . In a perpendicular field of  $B_{\perp} = 8$  T, the  $n_s/4$  state shifts towards lower  $|D|$ , the  $n_s/2$  state shifts towards higher  $|D|$ , and the  $3n_s/4$  state also emerges. In a parallel field of 8 T, on the other hand, the position of the states barely shifts but their resistance increases monotonically. (d-e) Resistance at the  $n_s/2$  correlated state versus displacement field, and magnetic field, for both (d) perpendicular and (e) in-plane to the device. While the correlated insulator state monotonically strengthens in  $B_{\parallel}$ , the perpendicular field induces a phase transition at around  $B_{\perp} = 5$  T, where the correlated state abruptly shifts to higher  $|D|$ . (f) In-plane magnetic field response of the correlated insulators at  $n_s/4$ ,  $n_s/2$  and  $3n_s/4$ . (g) Resistance of the  $n_s/2$  correlated state at an optimal  $|D|$  that maximizes its value, versus inverse temperature  $T^{-1}$  for different in-plane magnetic fields. The solid lines are fit to an Arrhenius behaviour  $\sim e^{-\Delta/2kT}$ . Inset shows  $\Delta$  obtained from the fitting for all three integer electron fillings versus  $B_{\parallel}$ . The  $g$ -factors extracted from these data are 0.52 for the  $n_s/2$  state, while being very small at 0.09 for  $n_s/4$  and  $3n_s/4$  states.

at  $n_s/4$ ,  $n_s/2$  and  $3n_s/4$  respectively, the gaps increase monotonically by applying an in-plane magnetic field, with effective  $g$ -factors of 0.09, 0.52 and 0.09 respectively. By comparison, similar experiments on TBGG<sup>23</sup>, have reported a  $g$ -factor close to 2 and attributed it to a possible purely

spin-polarized ground state for the  $n_s/2$  correlated state. While this argument does not apply to our data because the measured effective  $g$ -factors are much smaller than two, it is possible that the presence of disorder leads to a substantial underestimation of the gaps and their parallel magnetic field dependence. Alternatively, it is also possible that a mixed spin and valley polarization of the ground state has a reduced effective  $g$ -factor compared to a pure spin-polarized state. The monotonic increase in resistance with parallel magnetic field strongly suggest that the correlated insulator states have broken spin-rotation symmetry for all integer fillings, in stark contrast to the case of TBG, where the  $n_s/2$  insulator state resistance decreases both with  $B_\perp$  and  $B_\parallel$ <sup>1,2,9</sup>.

We note that all correlated insulator states in the  $\theta = 1.23^\circ$  TBBG device, whether at zero magnetic field or high magnetic fields, lie within the range  $D/\varepsilon_0 = -1.2 \text{ V nm}^{-1} \sim -0.4 \text{ V nm}^{-1}$ . Coincidentally, this is also the range where both the gap at charge neutrality ( $n = 0$ ) and the gap at the superlattice density ( $n = n_s$ ) are well-developed, as can be seen in Figs. 3a-c. Based on this observation, we suggest that the displacement field tunability of the correlated states is tied to the modulation of the single-particle band gaps by the displacement field. When either gap at  $n = 0$  or  $n = n_s$  is absent, the thermally excited or disorder scattered carriers from the upper or lower band would suppress the ordering of the electrons and hence the correlated states. Further theoretical developments are needed to reveal the detailed structure of the displacement field dependence of the correlated states.

We have also investigated the effect of substantially reducing the twist angle. Unlike the case of TBG, further reduction of the twist angle of TBBG to  $0.84^\circ$  results not only in one, but actually three pairs of flat bands, separated from other bands by band gaps (Fig. 4b). Application of an electrical displacement field further flattens these bands and separate them from each other (Fig. 4c). This would imply that all electrons within a density range  $-3n_s$  to  $+3n_s$  might experience strong Coulomb interactions, and their correlations can get further enhanced by applying a displacement field. These predictions from band theory are indeed consistent with our experimental observations. In Fig. 4a where we show the resistance map of the  $\theta = 0.84^\circ$  TBBG device versus  $n$  and  $D$ , we find weak signatures of  $-n_s/2$  and  $-n_s/4$  correlated insulator states only at high displacement fields  $|D|/\varepsilon_0 > 0.8 \text{ V nm}^{-1}$ . Noticeably, the full-filling gaps at  $\pm n_s$  and  $\pm 2n_s$  are also tunable by the displacement field to different extents. In Fig. 4d we apply a perpendicular magnetic field, and more correlated states are revealed similar to the spin-polarized states in the  $\theta = 1.23^\circ$  device. The strongest correlated states are observed at  $n/n_s = \pm \frac{1}{2}$ , and weaker states are visible at  $n/n_s = \frac{3}{2}$  and  $\frac{5}{2}$  in high magnetic fields. This is consistent with the fact that in Fig. 4c, the pair of bands closer to charge neutrality is flatter than the other two pairs of bands

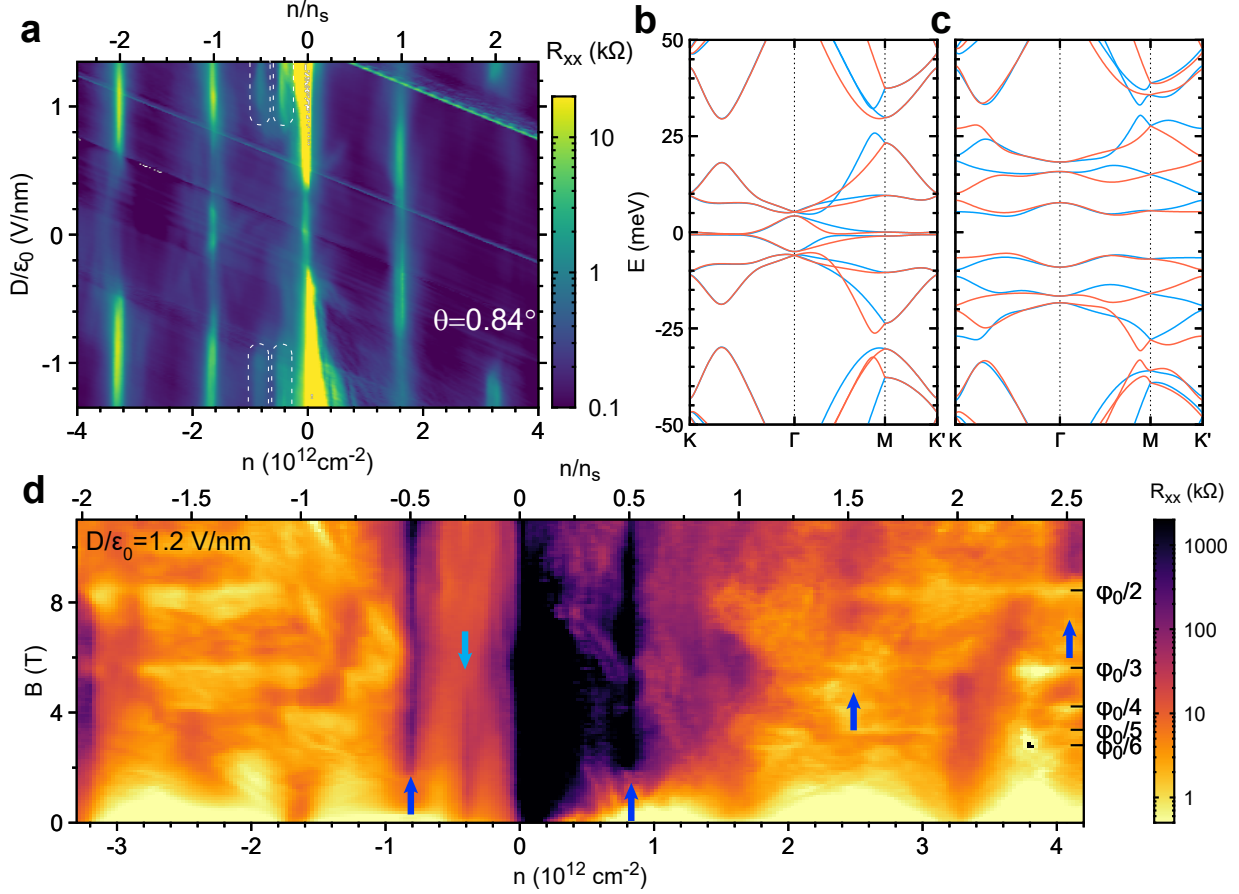


FIG. 4: Correlated insulator states in multiple flat bands. (a) Resistance map of a  $\theta = 0.84^\circ$  TBBG device. The top axis is the charge density  $n$  normalized to the superlattice density  $n_s$ . Besides the  $D$ -tunable gaps at multiples of  $n_s$ , we find signatures of correlated states at  $n/n_s = -\frac{1}{2}, -\frac{1}{4}$  at  $|D|/\epsilon_0 > 0.8$  V nm $^{-1}$ , which are labeled by dashed circles. (b-c) Calculated band structure of  $\theta = 0.84^\circ$  TBBG (b) without interlayer potential and (c) with interlayer potential  $\Delta V = 18$  mV. Near charge neutrality, within a 50 meV window, there are in total six sets of flat bands spanning densities  $-3n_s$  to  $3n_s$ . Upon applying a displacement field, these bands are further flattened and separated from each other, giving rise to correlated physics at each half-filling. (d) Resistance as a function of charge density and perpendicular magnetic field  $B$ . We observe strong correlated states at  $n/n_s = -\frac{1}{2}$  and  $\frac{1}{2}$ , and weaker states at  $\frac{3}{2}$  and  $\frac{5}{2}$  fillings. All the half-filling correlated states (indicated by dark blue arrows) are enhanced by the application of a magnetic field. The quarter-filling state at  $n/n_s = -\frac{1}{4}$  (indicated by the light blue arrow) is however suppressed by the magnetic field. Due to the formation of a superlattice, we also observe conductive features (bright horizontal features, see right axis) when  $B$  is such that the magnetic flux in each unit cell is equal to  $\varphi_0/2, \varphi_0/3, \varphi_0/4, \dots$ , where  $\varphi_0 = h/e$  is the flux quantum flux.

farther away from the charge neutrality. All correlated states at half-filling of these flat bands are enhanced by  $B$ , indicating at least partial spin-polarized ordering. The quarter-filling state at  $n/n_s = -\frac{1}{4}$ , on the other hand, appears to be spin-unpolarized. These results can open up a new route for studying electronic correlations in a multi-flat bands system.

Our results show that TBBG exhibits a rich spectrum of correlated phases tunable by twist angle, electric displacement field and magnetic field, paving the way to further studies of strongly correlated physics and topology in multi-flat band systems<sup>18</sup>.

---

\* [caoyuan@mit.edu](mailto:caoyuan@mit.edu)

† [pjarillo@mit.edu](mailto:pjarillo@mit.edu)

- <sup>1</sup> Cao, Y. *et al.* Correlated insulator behaviour at half-filling in magic-angle graphene superlattices. *Nature* **556**, 80–84 (2018).
- <sup>2</sup> Cao, Y. *et al.* Unconventional superconductivity in magic-angle graphene superlattices. *Nature* **556**, 43–50 (2018).
- <sup>3</sup> Bistritzer, R. & MacDonald, A. H. Moiré bands in twisted double-layer graphene. *Proceedings of the National Academy of Sciences* **108**, 12233–12237 (2011).
- <sup>4</sup> Lopes dos Santos, J. M. B., Peres, N. M. R. & Castro Neto, A. H. Continuum model of the twisted graphene bilayer. *Physical Review B* **86**, 155449 (2012).
- <sup>5</sup> Surez Morell, E., Correa, J. D., Vargas, P., Pacheco, M. & Barticevic, Z. Flat bands in slightly twisted bilayer graphene: Tight-binding calculations. *Physical Review B* **82**, 121407 (2010).
- <sup>6</sup> Carr, S. *et al.* Twistronics: Manipulating the electronic properties of two-dimensional layered structures through their twist angle. *Physical Review B* **95**, 075420 (2017).
- <sup>7</sup> McCann, E. & Koshino, M. The electronic properties of bilayer graphene. *Reports on Progress in Physics* **76**, 056503 (2013).
- <sup>8</sup> Castro Neto, A. H., Guinea, F., Peres, N. M. R., Novoselov, K. S. & Geim, A. K. The electronic properties of graphene. *Reviews of Modern Physics* **81**, 109–162 (2009).
- <sup>9</sup> Yankowitz, M. *et al.* Tuning superconductivity in twisted bilayer graphene. *Science* eaav1910 (2019).
- <sup>10</sup> Lu, X. *et al.* Superconductors, Orbital Magnets, and Correlated States in Magic Angle Bilayer Graphene. *arXiv:1903.06513 [cond-mat]* (2019). ArXiv: 1903.06513.
- <sup>11</sup> Sharpe, A. L. *et al.* Emergent ferromagnetism near three-quarters filling in twisted bilayer graphene. *arXiv:1901.03520 [cond-mat]* (2019). ArXiv: 1901.03520.
- <sup>12</sup> Chen, G. *et al.* Evidence of a gate-tunable Mott insulator in a trilayer graphene moiré superlattice. *Nature Physics* **15**, 237 (2019).
- <sup>13</sup> Chen, G. *et al.* Signatures of Gate-Tunable Superconductivity in Trilayer Graphene/Boron Nitride Moiré Superlattice. *arXiv:1901.04621 [cond-mat]* (2019). ArXiv: 1901.04621.
- <sup>14</sup> Dean, C. R. *et al.* Hofstadters butterfly and the fractal quantum Hall effect in moiré superlattices. *Nature* **497**, 598–602 (2013).
- <sup>15</sup> Kumar, R. K. *et al.* High-temperature quantum oscillations caused by recurring Bloch states in graphene superlattices. *Science* **357**, 181–184 (2017).

- <sup>16</sup> Hunt, B. *et al.* Massive Dirac Fermions and Hofstadter Butterfly in a van der Waals Heterostructure. *Science* **340**, 1427–1430 (2013).
- <sup>17</sup> Ponomarenko, L. A. *et al.* Cloning of Dirac fermions in graphene superlattices. *Nature* **497**, 594–597 (2013).
- <sup>18</sup> Zhang, Y.-H., Mao, D., Cao, Y., Jarillo-Herrero, P. & Senthil, T. Nearly flat Chern bands in moiré superlattices. *Physical Review B* **99**, 075127 (2019).
- <sup>19</sup> Cao, Y. *et al.* Superlattice-Induced Insulating States and Valley-Protected Orbits in Twisted Bilayer Graphene. *Physical Review Letters* **117**, 116804 (2016).
- <sup>20</sup> Kim, Y. *et al.* Charge Inversion and Topological Phase Transition at a Twist Angle Induced van Hove Singularity of Bilayer Graphene. *Nano Letters* **16**, 5053–5059 (2016).
- <sup>21</sup> Kim, K. *et al.* van der Waals Heterostructures with High Accuracy Rotational Alignment. *Nano Letters* **16**, 1989–1995 (2016).
- <sup>22</sup> Polshyn, H. *et al.* Phonon scattering dominated electron transport in twisted bilayer graphene. *arXiv:1902.00763 [cond-mat]* (2019). ArXiv: 1902.00763.
- <sup>23</sup> Kim, P. Ferromagnetic superconductivity in twisted double bilayer graphene, KITP Workshop on moiré physics (2019).

#### ACKNOWLEDGEMENTS

We acknowledge helpful discussions with S. Todadri, L. Fu, P. Kim, X. Liu, S. Fang and E. Kaxiras.